Advanced Multi-Channel SAR Imaging – Measured Data Demonstration

Nicolas Gebert, Felipe Queiroz de Almeida, Gerhard Krieger
Phone: +49 8153 / 28 -3331, Fax: +49 8153 / 28 -1449, Email: nico.gebert@dlr.de

Deutsches Zentrum für Luft- und Raumfahrt (German Aerospace Center), Microwaves and Radar Institute
P.O. Box 1116, 82234 Wessling, Germany

Abstract

Multi-channel synthetic aperture radar (SAR) allows for high-resolution wide-swath imagery thus overcoming the inherent limitation of conventional SAR. To cope with a non-uniformly sampled data array in azimuth caused by variations of the pulse repetition frequency (*PRF*), such systems require appropriate coherent processing as e.g. the multi-channel reconstruction algorithm. This paper presents the applicability of this algorithm to airborne measured multi-channel X-band data. In this context, impact and performance of different channel balancing methods are investigated. Furthermore, the analytic prediction of residual azimuth ambiguities is verified by the measured data by means of a point target analysis.

I. Introduction

A. Multi-Channel Reconstruction in Azimuth

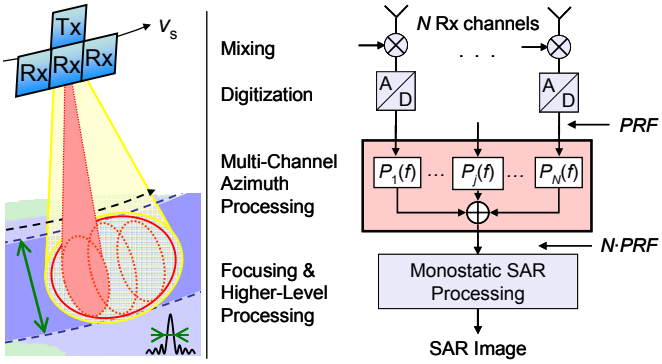

Fig. 1. Multi-channel SAR system for high-resolution wide-swath imaging (left) and corresponding block diagram with azimuth processing network (right).

Synthetic Aperture Radar (SAR) is a well-established technique for remote sensing of the Earth. However, conventional SAR systems with only a single transmit ("Tx") and receive ("Rx") aperture are not capable of imaging a wide swath with high spatial resolution [1]. Multi-channel SAR concepts, such as systems based on multiple Rx apertures in azimuth (cf. Fig. 1, left), promise to overcome these restrictions [2], [3]. As discussed in [2] and indicated in Fig. 1, right, additional signal processing by a suitable digital beamforming algorithm is required to deal with spatially unequally sampled multi-channel data. Such a "non-uniform" sampling in azimuth results from a mismatch between pulse repetition frequency (*PRF*) and Rx aperture positions. The optimum *PRF* value entailing uniform sampling is given in (1), where v_s is the sensor velocity, and N the number of adjacent Rx sub-apertures of size d_{az} each.

$$PRF_{\text{uni}} = \frac{2 \cdot v_s}{N \cdot d_{az}} \tag{1}$$

A suitable processing strategy is given by the "multi-channel reconstruction algorithm" [2]. It is based on an unambiguous recovery of the aliased azimuth spectrum, achieved by applying to each of the system's channels j, for a given *PRF*, a Doppler frequency f dependent filter function $P_{j,PRF}(f)$ (cf. Fig. 1, right). These functions are obtained by inverting a matrix, which is governed by the system geometry as derived in [2].

B. Residual Azimuth Ambiguities after Multi-Channel Reconstruction

As shown in [2], the processing network impacts the residual azimuth ambiguities, i.e. the azimuth-ambiguity-to-signal ratio in multi-channel systems depends on the weights $P_{j,PRF}(f)$ (cf. (2)). After reconstruction, the signal $S(f)$ in the denominator is governed by the normalized SAR signal $U(f)$ that corresponds to the azimuth signal envelope. $A_k(f)$ in the numerator defines the residual ambiguity of order k, where $U_k(f)$ is the *k-th* continuation of the signal spectrum after sampling, i.e. index k indicates a frequency shift by $k \cdot PRF$. $H_{jk}(f)$ basically describes the two-way path from transmitter to receiver j, and the functions $P_{jm,PRF}(f)$ finally represent the weighting by the processing filters. The azimuth system band $[-N \cdot PRF/2, N \cdot PRF/2]$ is decomposed into N sub-bands of width *PRF* which are specified by the index m. Starting with (2) and then considering the focusing allows for predicting the azimuth ambiguity-to-signal ratio after multi-channel processing.

$$\frac{A_k(f, PRF)}{S(f)} = \frac{U_k(f) \cdot \sum_{m=1}^{N} \sum_{j=1}^{N} H_{jk}(f) \cdot P_{jm,PRF}(f)}{N \cdot U(f)} \tag{2}$$

II. Reconstruction of Airborne Measured Multi-Channel Data

A. Multi-Channel F-SAR Data

German Aerospace Center's (DLR) state-of-the art airborne sensor F-SAR allows for the simultaneous acquisition of multiple along-track channels [4]. In X-band, a single Tx antenna can be combined with four Rx antennas operated in two receiver chains. In consequence, two channels each are switched continuously from pulse to pulse yielding two pairs of alternately acquired channels (cf. Fig. 2). The offset between the Rx antennas is defined by their dimensions of d_{az} = 0.2 m each, leading in a first step to an effective phase center spacing of 0.1 m. The switching by a transmit *PRF* of 5 kHz in combination with a sensor velocity of 91 m/s results in an additional along-track offset of ~2 cm between alternated receivers. As a result, four channels sampled at 2.5 kHz each and with the effective phase center distances given in Fig. 2 are obtained.

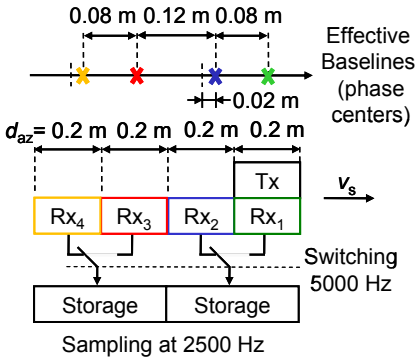

Fig. 2. F-SAR antenna geometry and acquisition setup leading to four azimuth channels. The "Storage" block summarizes down-conversion, digitization and storage of the data.

In the following, multi-channel data acquired over the runway of an airport close to Memmingen (Bavaria) will be analyzed. A first proof-of-principle of the algorithm's applicability to this data set has been given in [4], where two channels were combined. As a next step, up to four channels are combined and focus is turned to the investigation of different channel balancing methods and their capability to compensate for channel mismatches. Furthermore, the prediction of the residual azimuth ambiguities as derived in Section I.B is verified by the reconstruction results of the measured data.

B. Sub-Sampling, Multi-Channel Reconstruction and Signal Processing

As focus is on azimuth dimension, motion compensated and range compressed data are considered. Since the data show high oversampling in azimuth, preliminary processing steps are required to generate aliased channels.[1] According to the processing scheme of Fig. 3, this is achieved by band-limiting the data in azimuth to a bandwidth of B_{az}, followed by decimation leading to a reduced sampling rate PRF_{eff} according to the decimation factor. Band limitation and decimation are adjusted to obtain sub-sampling in each of the N channels but to ensure Nyquist-sampling for the combination of all channels, i.e. $N{\cdot}PRF_{eff} = B_{az}$. In the present case, B_{az} = 625 Hz and K_d = 4 are chosen. Consequently, as shown in Fig. 3 on the left, each input channel is decimated by a factor of $N{\cdot}K_d$. In a next step, the N aliased channels are combined by the multi-channel reconstruction algorithm, yielding a single output channel of effective sampling $N{\cdot}PRF_{eff}$. In addition, a reference image without aliasing – representing the ideal output of the reconstruction – and the image obtained from an aliased single channel are presented. All data are focused using the conventional monostatic Range Doppler Algorithm (RDA). Note that this includes the range cell migration correction (RCMC), as phase errors introduced in the reconstruction by the RCM are negligible in this geometry.

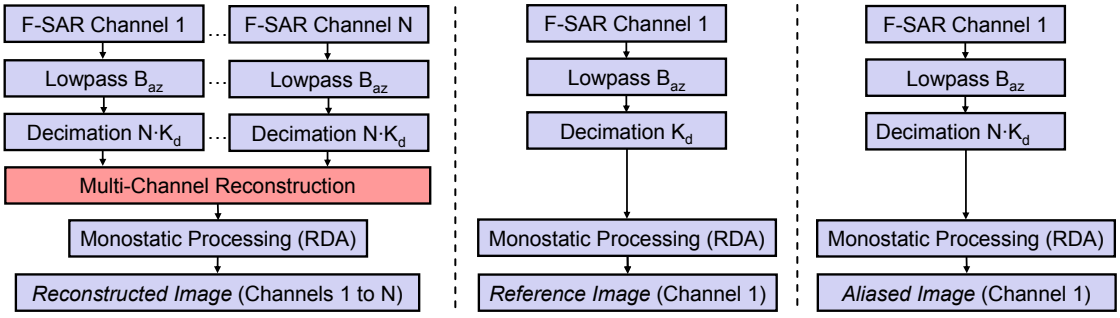

Fig. 3. Block diagram summarizing input data generation and SAR processing for different cases: reconstruction of multi-channel data (left), ideal monostatic reference (middle) and image for a single aliased channel (right).

The relevant parameters for the airborne data and the processing are summarized in Table. 1. In the following, the combinations of two and four channels, respectively, are analyzed. The corresponding spatial sample distribution in azimuth is illustrated in Fig. 4, where one recognizes for both scenarios a clearly non-uniform sampling.[2]

[1] Azimuth ambiguities are a limiting factor to spaceborne high-resolution wide-swath SAR [2]. In contrast, airborne SAR data are in general not affected by azimuth ambiguities. Thus, for reasons of demonstration, the ambiguities have to be "generated" artificially.

[2] Both scenarios are defined to show the same output *PRF* after multi-channel reconstruction. Since decimation varies with the number of channels, the respective single-channel *PRF* is different for the two considered cases.

Parameter	Symbol	Value
Carrier frequency	λ/c_0	9.65 [Hz]
Platform velocity	v_s	91.0 [m/s]
Sensor height	h_s	2150 [m]
Operational PRF	PRF_0	2500 [Hz]
Azimuth Bandwidth	B_{az}	625 [Hz]
Processed Doppler Bandwidth	B_d	365 [Hz]
Processed Doppler centroid	f_{dc}	130 [Hz]
Number of channels	N	2, 4

Table. 1. Relevant system and processing parameters.

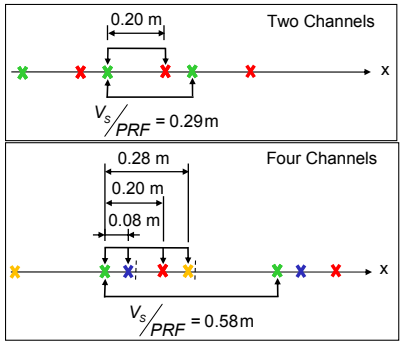

Fig. 4. Azimuth spatial sampling for N=2 (top) and N=4 (bottom).

The results for N=2 channels are presented in Fig. 5. Left shows the SAR reference image free of ambiguities (top) and the slice of the azimuth impulse response of the corner reflector located on the runway (bottom). Middle presents the aliased single channel resulting in degraded resolution δ_{az} and a strongly ambiguous image. For the corner reflector, the mean peak level of the ambiguities – marked by the circles – is 15.3 dB below the signal peak. Finally, the image obtained from the reconstruction of two aliased channels is given on the right, showing clearly improved azimuth resolution and ambiguity suppression, with residual mean ambiguity-to-signal peak level dropped to -35.6 dB.

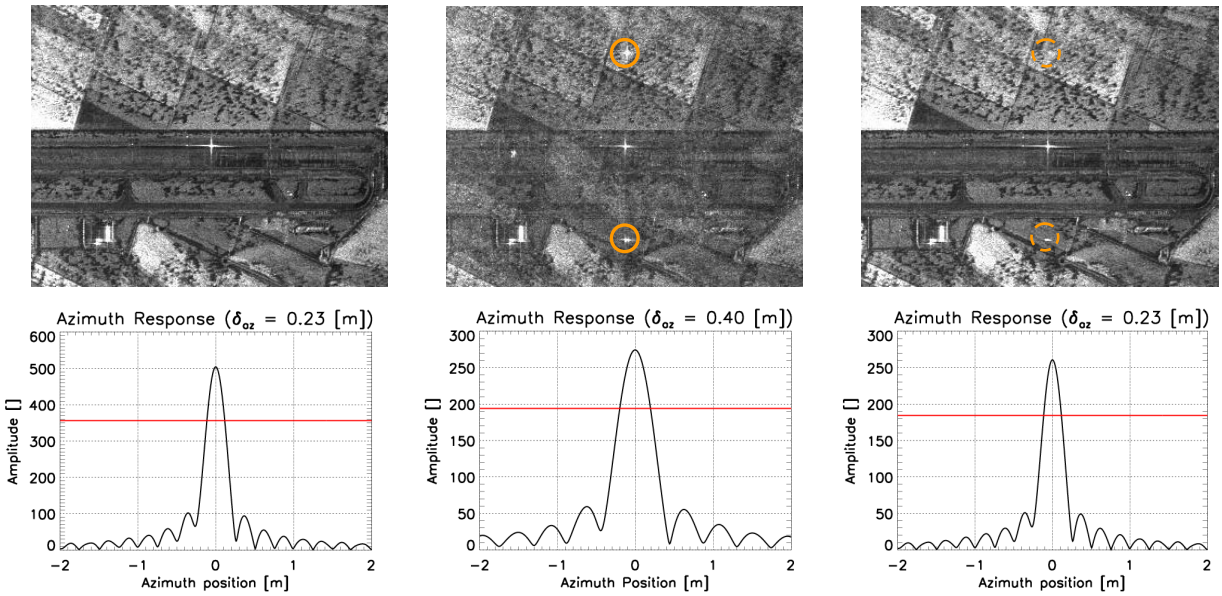

Fig. 5. Reference (left), aliased (middle) and reconstructed (right) images (top) and azimuth slices (bottom), for the combination of N=2 channels.

C. *Channel Balancing for Improved Multi-Channel Reconstruction*

In a multi-channel system different Rx hardware causes gain and phase imbalances. In practice, this introduces “unknown” differences between the channels, which are not considered by the multi-channel processing. As reported above, this leads to residual azimuth ambiguities demanding for balancing the channels.

An effective method for such a channel balancing is given by the “2D Adaptive Calibration”, which is applied in range Doppler domain and follows the rationale that remaining differences between well calibrated channels are only due to their along track displacement [5]. Consequently, the technique removes as a preliminary step the phase ramp due to baseline (“co-registration”), followed by an iterative minimization of the integral of the square calibration error. In a second approach, the “2D Adaptive Calibration” strategy may be complemented by the additional removal of a box-car averaged phase difference in time domain (“Averaging Window Method”) [6], [7], accounting for the removal of cross-track baseline components and residual imbalances. Note that – since the along-track baseline information needs to be preserved in the reconstruction context – the detected phase ramp has to be re-introduced after calibration.

Applying in a first step the proposed channel balancing methods to the fully sampled data before decimation in azimuth, one obtains for the reconstruction of N=2 channels the results summarized in Fig. 6. Without any calibration (left), the mean peak ambiguity level is -35.6 dB compared to the target peak and the ambiguities marked by the circles are still visible. After the 2D Adaptive Calibration (middle), this value drops to -

39.8 dB, meaning they are hardly noticeable, and after the cascade (left), to -41.5 dB, with virtually inexistent ambiguities. Hence, the compensation of channel imbalances – especially with regard to phase – clearly improves the ambiguity suppression. The additional application of the Averaging Window method entails a further improvement as it removes residual imbalances in the output of the 2D Adaptive Calibration. The azimuth slices of the corner reflector are not shown explicitly as they have all the same appearance.

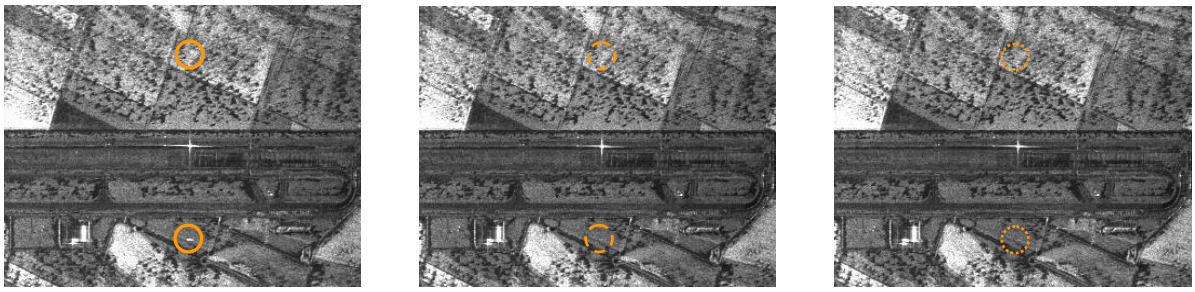

Fig. 6. Reconstructed images of N=2 channels without calibration (left), after 2D Adaptive Calibration (middle) and after the cascade of the 2D Adaptive Calibration and the Averaging Window method (right).

In comparison to the two channels reconstructed above, the other channels show a larger phase imbalance, consisting not only but primarily of a constant phase difference. This is the reason for the poor reconstruction result when all four channels are combined without calibration, as shown in Fig. 7 on the left. Applying the cascade of 2D Adaptive Calibration and Averaging Window method leads to a clear improvement; visually as well as in terms of resolution δ_{az} and a mean ambiguity level of -39.9 dB (cf. Fig. 7, right).

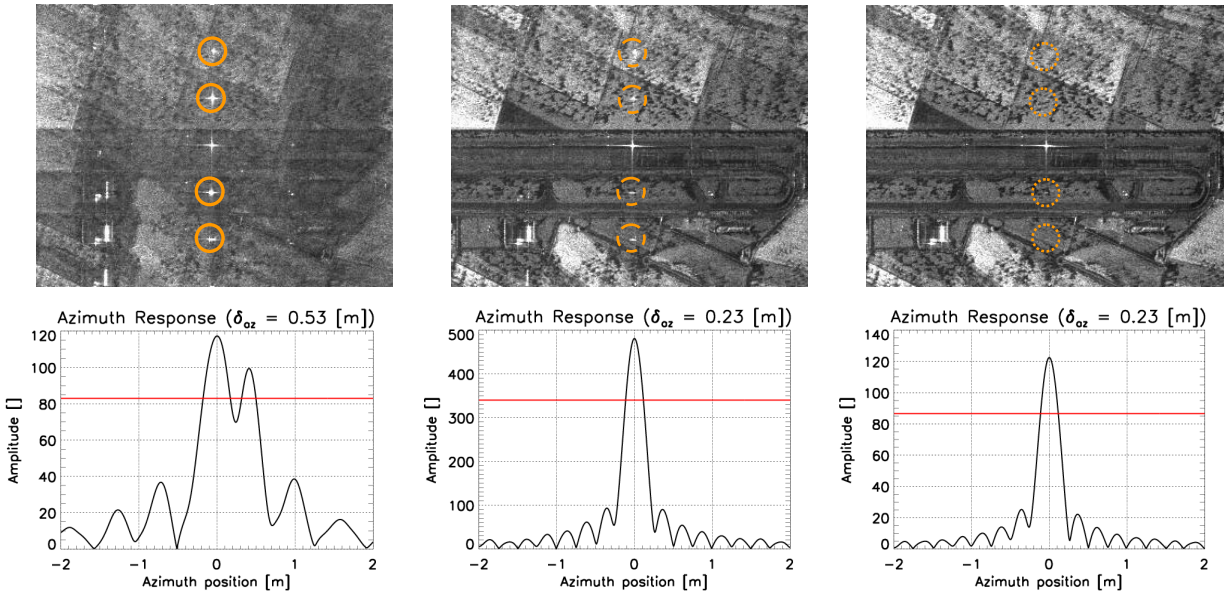

Fig. 7. Reconstructed images of N=4 channels without calibration (left), after histogram based phase correction (middle) and complete calibration scheme, i.e. 2D Adaptive Calibration followed by Averaging Window method (right).

So far, calibration has been applied to the non-ambiguous signals before decimation, while in a real system only sub-sampled channels are available which cause the 2D Adaptive Calibration to fail.

Based on the perception that channel imbalances are dominated by a constant phase offset, two different approaches applicable to sub-sampled data are presented as follows. After removing the expected baseline, the first method performs in range Doppler domain – extended to the full system band $N{\cdot}PRF_{\text{eff}}$ – a histogram analysis of the interferometric phase between the channels. Then the histogram's maximum gives the phase offset to be corrected for the respective channel, leading to the reconstruction as shown in Fig. 7, middle, with a mean ambiguity level of -31.6 dB and a much improved aspect. This method turned out to yield virtually the same result as the time domain calibration algorithm employed in [8], if additionally a possible Doppler centroid is considered. This is necessary to resolve a possible ambiguity of the estimated phase caused by the sub-sampling of the individual channels. In either case, residual phase imbalances remain, explaining the difference to the case after full calibration of the data before decimation.

The quantitative analysis of the residual ambiguities after coherent combination for different balancing methods highlights the sensitivity of the algorithm to phase errors introduced by channel imbalances, which may be – although not completely removed – clearly attenuated using the sub-sampled data. Given balanced channels, the reconstructed images are virtually indistinguishable from the reference.

D. Residual Azimuth Ambiguities – Prediction and Measurement

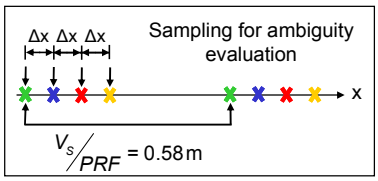

Fig. 8. Imposed sampling, N=4.

Section I.B presented an analytical prediction of the residual ambiguity levels depending on the spatial sampling conditions. The predicted behavior shall be verified by imposing a varying inter-element spacing Δx to the four measured channels (cf. Fig. 8), where the respective shift is obtained by interpolation of the fully sampled data. Afterwards, the channels are reconstructed according to Fig. 3, but without band limitation to cause inherent sub-sampling in the recovered image. Further, B_D is increased to 625 Hz. After focusing, the residual ambiguities of the corner reflector are evaluated with respect to their peak power. The measurements (cf. Fig. 9, solid lines) are compared to the simulated prediction ('+' symbols), obtained by means of a point target response which takes into account the acquisition geometry, parameters and azimuth pattern. Ambiguities up to the fourth order are considered, showing accurate match in the regions where the ambiguities are not masked by scene background or noise. For the "intermediate" ambiguities of order 1 to N-1, one clearly recognizes the minimum at the optimum spacing of $v_s/(PRF \cdot N)$ = 14.5 cm, and the degradation for a spacing deviating from this value. In contrast, the first "regular" ambiguity, i.e. order N, remains constant independent of the spacing (cf. Fig. 9, right).

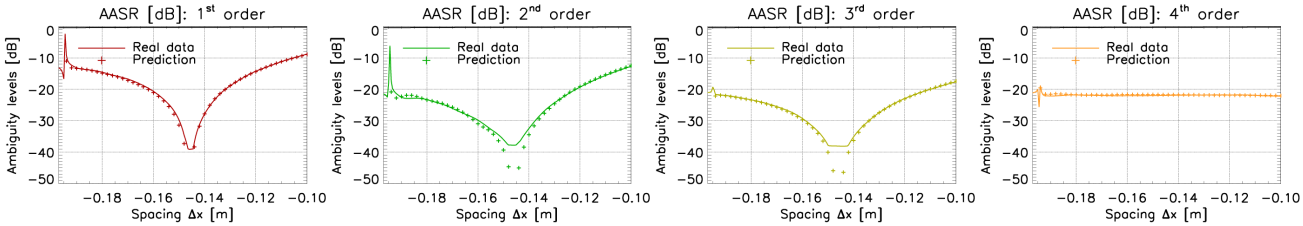

Fig. 9. Comparison of predicted ('+' symbols) and measured (solid lines) peak ratios of azimuth ambiguities to signal. Ambiguities of order 1 to 3 vary strongly with the sample spacing, while "regular" ambiguity of order N remains constant.

III. Summary

The paper demonstrates the applicability of the multi-channel reconstruction algorithm to measured multi-channel X-band data. Up to four individual receiving channels, each sub-sampled, were combined to a single channel, ideally free of aliasing but in reality showing residual azimuth ambiguities caused by channel imbalances. Consequently, different channel balancing methods were presented, demonstrating improved ambiguity suppression. In a first step, channel balancing was applied to the data before decimation, in order to show the impact of channel imbalances and to allow for a comparison of different approaches. As these Doppler domain methods fail when applied to sub-sampled data after decimation, a second step derived a new channel balancing approach applicable to aliased data. This histogram-based method in range-Doppler allows for compensating a constant phase offset which represents the main cause of imbalances, by this enabling a clearly better balancing and improved reconstruction results. The approach is comparable to a time domain synchronization method [8], after a squint-angle pointing adaptation to account for the Doppler centroid. Based on these promising results, future work will further elaborate channel balancing techniques for sub-sampled data in order to derive suitable calibration strategies for future multi-channel systems.

References

[1] J. Curlander and R. McDonough, *Synthetic Aperture Radar – Systems and Signal Processing*, J. Wiley & Sons, 1991.

[2] N. Gebert, G. Krieger, and A. Moreira, "Digital Beamforming on Receive: Techniques and Optimization Strategies for High-Resolution Wide-Swath SAR Imaging", *IEEE Trans. Aerosp. Electron. Syst.*, vol. 45 (2), pp. 564-592, 2009.

[3] G. Krieger, N. Gebert, and A. Moreira, "Multidimensional Waveform Encoding: A New Digital Beamforming Technique for Synthetic Aperture Radar Remote Sensing", *IEEE Trans. Geosci. Remote Sens.*, vol. 46 (1), pp. 31-36, 2008.

[4] S. Baumgartner, et al., "Digital Beamforming and Traffic Monitoring Using the new F-SAR System of DLR", *Proceedings of International Radar Symposium* (*IRS*), Cologne, Germany, 2007.

[5] C.H. Gierull, "Digital Channel Balancing of Along-Track Interferometric SAR Data", Technical Memorandum, DRDC Ottawa, 2003.

[6] R. Lanari, et al., "Generation of digital elevation models by using SIR-C/X-SAR multifrequency two-pass interferometry – The Etna case study", *IEEE Trans. Geosci. Remote Sens.*, vol. 34 (5), pp 1097-1114, 1996.

[7] L. Yang, T. Wong and Z. Bao, "Ground Moving Target Indication using an In-SAR System with a hybrid baseline", *IEEE Geosci. Remote Sens. Lett.*, vol. 5 (3), pp. 373-377, 2008.

[8] J. Kim, A. Ossowska, W. Wiesbeck, "Experimental investigation of Digital Beamforming SAR performance using a ground-based demonstrator", *Proceedings of International Geoscience and Remote Sensing Symposium* (*IGARSS*), Barcelona, Spain, 2007.